High Efficiency Injectorless Quantum Cascade Lasers Emitting at 8.8 μm with 2 W Peak Pulsed Power per Facet at Room Temperature

H. Li, Simeon Katz, *Member, IEEE,* Augustinas Vizbaras, *Graduate Student Member, IEEE,* Gehard Boehm, and Markus-Christian Amann, *Fellow, IEEE*

***Abstract*—An injectorless quantum cascade laser (QCL) design using four material alloys and emitting around 8.8 μm at room temperature is presented. The coupling energy between the injection state and the upper laser level was increased compared to other injectorless designs to 10.6 meV. Devices with 85 repeats produce 2.0 W of pulsed output power per facet and an overall efficiency of 7.2% at 300 K. The threshold current density at room temperature is as low as 1.15 kA/cm^2 for an as-cleaved 4 mm long device, with a characteristic temperature of 162 K.**

***Index Terms*—injectorless, mid infrared, quantum cascade lasers, semiconductor lasers.**

I. Introduction

WITHIN the last years injectorless quantum cascade lasers [1] significantly improved regarding threshold current density [2], [3] and output power [4] as well as overall efficiency [4], [5]. However, the output power and the wall-plug efficiency at room temperature have still been falling short [3]–[5] compared to injector-based quantum cascade lasers [6], [7] of similar wavelength. In theory, the injectorless device requires less voltage per period and allows more transitions within the same thickness of the active region, offering higher voltage efficiency and low threshold current densities. The overall efficiency can be derived as [8]

$$\eta_{\mathrm{wp}} = \frac{j_{\max} - j_{\mathrm{th}}}{j_{\max}} \frac{\alpha_{\mathrm{m}}}{\alpha_{\mathrm{m}} + \alpha_{\mathrm{i}}} \frac{E_{\mathrm{ph}}}{E_{\mathrm{ph}} + eV_{\mathrm{def}} + eIR_{\mathrm{s}}/N_{\mathrm{p}}} \eta_{\mathrm{tr}} \qquad (1)$$

with $j_{\max}$ and j_{th} being the maximum and the threshold current density. N_{p}, α_{m}, and α_{i} denominate the number of periods, the mirror losses and the internal losses accordingly. η_{tr} is the differential efficiency of the laser transition. The voltage efficiency is determined by the energy per photon E_{ph}, the voltage defect eV_{def}, used for depletion and injection, as well as the serial resistance R_{s}. Injectorless designs exhibit theoretically a higher efficiency, due to their smaller threshold current densities as well as their lower voltage defects. Here, one point should be noted; while reducing eV_{def} will significantly increase the wall-plug efficiency, that occurs mostly at cryogenic temperatures. Close to and at room temperature the reduction in eV_{def} causes significant increases in the backfilling current, which in turn increases j_{th} and causes low-eV_{def} devices to have the same or lower room temperature wall-plug efficiencies than conventional eV_{def} devices [9]. The shorter period does not only improve the threshold current density but also increases the electric fields during operation. This reduces the injection efficiency and lifetimes towards short wavelengths, counteracting the possible improvements by the more compact design. Therefore injectorless devices tend to be more efficient compared to injectorbased devices towards longer wavelengths. Long wavelength devices are not only demanded for sensing applications [10] and communication [11] within the atmospheric transmission window but also for THz emission by intracavity difference frequency generation [12].

Manuscript received July 21, 2010; revised September 30, 2010; accepted October 02, 2010.

The authors are with the Walter Schottky Institut, Technische Universität München, Am Coulombwall 3, D-85748 Garching, Germany (e-mail: Hua.Li@wsi.tum.de, simeon.katz@osram-os.com).

II. Design, processing and characterization

In this work, we present results from a modified design based on the first four-alloy injectorless design [2]. Figure 1 shows this design, using a blocking barrier with AlAs, and an InAs-enhanced well for the optical transition. The transition was shifted to be more diagonal compared to the original design, decreasing the dipole matrix element from 1.4 to 1.1 nm and increasing the upper state lifetime from 3.7 to 5.66 ps at resonance. Additionally, the coupling energy [13] was increased from 5.7 to 10.6 meV by reducing the injection barrier thickness from 2.5 to 1.9 nm. The design

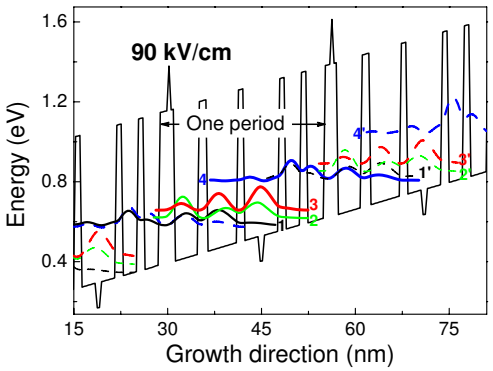

Fig. 1. Subsequent periods of the injectorless active region design using four different material alloys, strain-balanced on InP. State 4 indicates the upper laser level, while state 3 shows the lower laser level and state 1 and 2 are used for resonant phonon depletion.

field decreased from 103 to 88 kV/cm reducing the simulated transition energy from 178 to 144 meV. Additionally the barriers between the depletion states were increased by 10% to suppress current flow below the designed resonance. The layer sequence of the 25.9 nm long period is given by (in nm): **1.0**/***0.4***/**0.5**/4.1/**1.2**/5.1/**1.0**/2.4/*0.51*/2.5/**0.9**/2.6/**1.0**/2.7, with ***bold italic layers*** identifying AlAs, **bold layers** for AlInAs, regular layers for GaInAs and *italic ones* indicating the InAs. The underlined layers were silicon doped to a corresponding doping sheet density of 4.5×10^{10} cm^{-2}.

The sample was grown in a solid source molecular beam epitaxy (MBE) starting with a 500 nm thick InGaAs cladding, lattice matched to InP and doped to 6.0×10^{16} cm^{-3}, followed by the 85-stages active region with a total thickness of 2.20 μm and then capped by another 500 nm thick InGaAs cladding. The upper waveguide consists of a 2.7 μm thick InP layer being doped 6.0×10^{16} cm^{-3} and a 1.2 μm thick top cap of InGaAs doped to 5.0×10^{18} cm^{-3} and 1.0×10^{19} cm^{-3} for the last 200 nm.

The chip processing was done with chlorine reactive ion etching to form mesa stripes between 22 μm and 30 μm in width. Afterwards a silicon-dioxide passivation including dry-etched contact windows and regular Ti/Pt/Au contacts was formed. The mounting was done with as-cleaved Fabry-Pérot lasers episide-up on copper heat sinks.

For measuring the power, a calibrated thermopile detector was used, while running the lasers at 10 kHz with a duty cycle of 0.5%. The power data, presented here, therefore corresponds simply to the measured power divided by the duty cycle and corrected for 70%±0.05 collection efficiency. The spectrum was recorded with a Bruker Fourier transform infrared (FTIR) spectrometer (Vertex70), while threshold measurements were performed using a liquidnitrogen-cooled cryostat and a mercury-cadmium-telluride detector setup. Threshold current densities over temperature were determined using 500 ns long pulses and a duty cycle of 0.0125%.

III. Results and discussion

The threshold and the slope efficiency over temperature behaviour for an uncoated 4 mm long device are shown in Fig. 2. At 300 K the pulsed threshold current density was measured to be 1.15 kA/cm^2 while the characteristic temperature for j_{th}, T_0, is 162 K indicating a small degree of carrier leakage. The larger threshold current density compared to the previous structures [2] emitting around 7.1 μm is attributed to increased waveguide losses. The characteristic temperature for the slope efficiency T_1 shows four different values in the temperature range of 78-400 K. Around room temperature T_1 is 108 K. Though the value is lower than that reported for deep-well design QCLs, it is comparable to T_1 of a high efficiency QCL emitting at 4.6 μm [14]. The inset of Fig. 2 shows the low-temperature spectrum at high currents and the room temperature spectrum close to threshold. The maximum temperature of operation was 400 K for a 4 mm long device. The waveguide loss and gain coefficient were determined from devices differing in length to be 9±1 cm^{-1} and 17 cm/kA at room temperature, respectively. This yields a

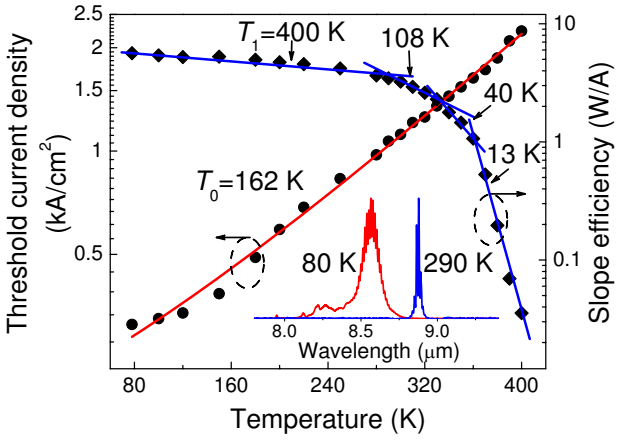

Fig. 2. Threshold current density and slope efficiency versus temperature for an as-cleaved 4 mm long and 30 μm wide laser. Characteristic temperatures T_0 for j_{th} and T_1 for slope efficiency are shown. The inset shows the normalized emission spectra at 80 and 290 K.

theoretical slope efficiency between 3.0 and 3.5 W/A for both facets, in good agreement with the experimental result.

The *L-I-V* curves together with the overall efficiency are given in Fig. 3. The maximum output power at 300 K was measured to be 1.95 W with a slope efficiency of 1.7 W/A per facet for an uncoated device, taking the collection efficiency of 70% into account. The overall efficiency is taken from the front facet power being doubled (for uncoated devices) and corrected for the serial resistance (≈0.9 Ω) of the cryostat wiring. The overall efficiency was measured to be 22% and 7.2% at 78 K and 300 K, respectively. These values show that injectorless devices can be as efficient as injectorbased devices within the 8 to 12 μm wavelength range. Additionally they have a much lower voltage defect with 56 meV corresponding to a voltage efficiency of 66% in comparison to injectorbased devices with a typical voltage defect of 110 meV [7] and

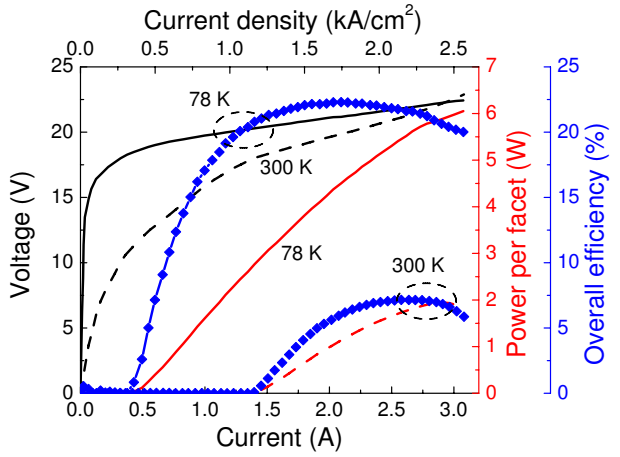

Fig. 3. Optical output power per facet, voltage and overall efficiency over current for a 4 mm long and 30 μm wide device. The voltage is given by the black solid (78 K) and dashed (300 K) lines, while the output power is given by the red solid (78 K) and dashed (300 K) lines. The overall efficiency is indicated by blue scatters.

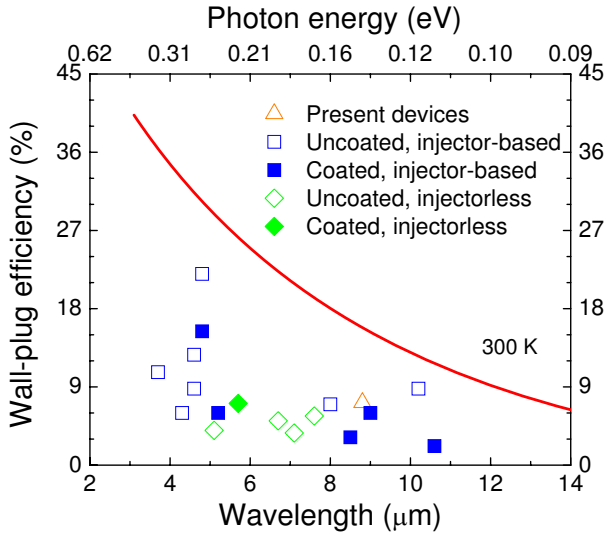

Fig. 4. Comparison of overall efficiency for injectorbased (blue, squares) and injectorless devices (green, diamonds) around 300 K. The efficiency of the present devices is given by an orange triangle. The solid theoretical line of efficiency versus wavelength is taken from reference [8].

a corresponding voltage efficiency of only 51%. It is worth noting that though Eq. (1) assumes that η_{wp} reaches its maximum at $j=j_{max}$, the measured pulsed *L-I* curves bend at high currents which in turn causes the maximum in η_{wp} to occur at currents below j_{max} as shown in Fig. 3.

Figure 4 shows a comparison of overall efficiency at room temperature for injectorless and injectorbased devices. The line shows a theoretical result [8], while experimental results are represented by scatters. The highest efficiency achieved so far is 22% [15]. According to Eq. (1), Fig. 4 shows that the η_{wp} values of back facet, high-reflectivity coated devices are smaller than those for uncoated devices. Current experimental results are still far away from the theoretical prediction leaving considerable space for the improvement in wall-plug efficiency.

The significantly improved performance of the present devices compared to previous injectorless QCLs [2], [4] is due to: (1) Enhanced injection coupling. The injection coupling strength directly determines the tunneling rate, the modal gain, j_{max}, η_{wp} and many other performance-related parameters. Furthermore, in this device the upper lasing state is designed to be a single state rather than a double-resonant state in previous designs. So the injection efficiency is further improved, and the upper state lifetime gets as high as 5.66 ps. (2) Improved MBE material quality. Extensive work has been done in the material growth especially for four- or five-alloy active region structures to reduce the interface roughness yielding a significantly improved crystal quality. (3) The increased number of periods from 60 to 85 also contributes to the high output pulsed power.

IV. Summary

In summary, we have shown an injectorless design using multiple alloys, a stronger injection coupling and a more diagonal transition to increase the power efficiency in pulsed mode. We have also proven that injectorless devices can be as efficient as injectorbased devices [7], [15], [16] at long wavelengths, while exhibiting lower threshold current densities and higher output pulsed powers.

Acknowledgment

The authors gratefully acknowledge the financial support by the German excellence cluster “nanosystems initiative Munich (NIM)”. One of the authors (H.L.) acknowledges the support from the Alexander von Humboldt foundation.

References

[1] M. C. Wanke, F. Capasso, C. Gmachl, A. Tredicucci, D. L. Sivco, A. L. Hutchinson, S. N. G. Chu, and A. Y. Cho, “Injectorless quantum-cascade lasers,” *Appl. Phys. Lett.*, vol. 78, pp. 3950-3952, Jun. 2001.

[2] S. Katz, G. Boehm, and M. C. Amann, “Low-threshold injectorless quantum cascade laser with four material compositions,” *Electron. Lett.*, vol. 44, pp. 580-581, Jun. 2008.

[3] G. Boehm, S. Katz, R. Meyer, and M. C. Amann, “Al(In)As-(Ga)InAs strain-compensated active regions for injectorless quantum cascade lasers,” *J. Cryst. Growth*, vol. 311, pp. 1932-1934, Mar. 2009.

[4] S. Katz, A. Vizbaras, G. Boehm, and M. C. Amann, “High-performance injectorless quantum cascade lasers emitting below 6 μm,” *Appl. Phys. Lett.*, vol. 94, pp. 151106-1-151106-2, Apr. 2009.

[5] Y. B. Bai, S. Slivken, S. Kuboya, S. R. Darvish, and M. Razeghi, “Quantum cascade lasers that emit more light than heat,” *Nature Photonics*, vol. 4, pp. 99-102, Feb. 2010.

[6] A. Lyakh, R. Maulini, A. Tsekoun, R. Go, C. Pflugl, L. Diehl, Q. J. Wang, F. Capasso, and C. K. N. Patel, “3 W continuous-wave room temperature single-facet emission from quantum cascade lasers based on nonresonant extraction design approach,” *Appl. Phys. Lett.*, vol. 95, pp. 141113-1-141113-3, Oct. 2009.

[7] Q. J. Wang, C. Pflugl, L. Diehl, F. Capasso, T. Edamura, S. Furuta, M. Yamanishi, and H. Kan, “High performance quantum cascade lasers based on three-phonon-resonance design,” *Appl. Phys. Lett.*, vol. 94, pp. 011103-1-011103-3, Jan. 2009.

[8] J. Faist, “Wallplug efficiency of quantum cascade lasers: Critical parameters and fundamental limits,” *Appl. Phys. Lett.*, vol. 90, pp. 253512-1-253512-3, Jun. 2007.

[9] P. Q. Liu, A. J. Hoffman, M. D. Escarra, K. J. Franz, J. B. Khurgin, Y. Dikmelik, X. J. Wang, J. Y. Fan, and C. F. Gmachl, “Highly power-efficient quantum cascade lasers,” *Nature Photonics*, vol. 4, pp. 95-98, Feb. 2010.

[10] A. A. Kosterev and F. K. Tittel, ”Chemical sensors based on quantum cascade lasers,” *IEEE J. Quantum Electron.*, vol. 38, pp. 582-591, Jun. 2002.

[11] R. Martini and E. A. Whittaker, “Quantum cascade laser-based free space optical communications,” *J. Opt. Fiber Commun. Res.*, vol. 2, pp. 279-292, 2005.

[12] M. A. Belkin, F. Capasso, A. Belyanin, D. L. Sivco, A. Y. Cho, D. C. Oakley, C. J. Vineis, and G. W. Turner, “Terahertz quantum-cascade-laser source based on intracavity difference-frequency generation,” *Nature Photonics*, vol. 1, pp. 288-292, May 2007.

[13] J. B. Khurgin, Y. Dikmelik, P. Q. Liu, A. J. Hoffman, M. D. Escarra, K. J. Franz, and C. F. Gmachl, “Role of interface roughness in the transport and lasing characteristics of quantum-cascade lasers,” *Appl. Phys. Lett.*, vol. 94, pp. 091101-1-091101-3, Mar. 2009.

[14] J. C. Shin, M. D’Souza, Z. Liu, J. Kirch, L. J. Mawst, D. Botez, I. Vurgaftman, and J. R. Meyer, “Highly temperature insensitive, deep-well 4.8 μm emitting quantum cascade semiconductor lasers,” *Appl. Phys. Lett.*, vol. 94, pp. 201103-1-201103-3, May 2009.

[15] M. Razeghi, S. Slivken, Y. B. Bai, B. Gokden, and S. R. Darvish, “High power quantum cascade lasers,” *New J. Phys.*, vol. 11, pp. 125017-1-125017-13, Dec. 2009.

[16] A. Vizbaras, S. Katz, G. Boehm, and M. C. Amann, “Short-Injector Quantum Cascade Laser Emitting at 8-μm Wavelength With High Slope Efficiency,” *IEEE Photonics Technol. Lett.*, vol. 21, pp. 1384-1386, Oct. 2009.